Journal of COMPUTATIONAL CHEMISTRY WWW.C-CHEM.ORG FULL PAPER

Geometric Analysis of Anharmonic Downward Distortion Following Paths

Shuichi Ebisawa,[1] Takuro Tsutsumi,[1] and Tetsuya Taketsugu[2,3]

Correspondence to: Tetsuya Taketsugu (E-mail: take@sci.hokudai.ac.jp)

[1] *Graduate School of Chemical Sciences and Engineering, Hokkaido University, Sapporo 060-0810, Japan*
[2] *Department of Chemistry, Faculty of Science, Hokkaido University, Sapporo 060-0810, Japan*
[3] *Institute for Chemical Reaction Design and Discovery (WPI-ICReDD), Hokkaido University, Sapporo 001-0021, Japan*

ABSTRACT

A mathematical aspect of the anharmonic downward distortion following (ADDF) path is discussed. The ADDF method is utilized as an automated reaction path search method, which can explore transition state geometries on a potential energy surface from a potential minimum. We show that the maximum number of the ADD stationary paths intersecting the potential minimum is $2^{f+1}-2$, where f denotes the degree of freedom of the system. We also show that the bifurcation of the ADD stationary path is essential to detect all the transition states connected from a given minimum. The ADDF computation is demonstrated for a H_2O molecule in which pitchfork bifurcation is observed.

Introduction

Reaction path concept has played a significant role in the theoretical study of chemical reactions. As a representative reaction path, Fukui introduced the intrinsic reaction coordinate (IRC),[1,2] which is defined as the steepest descent path from the transition state (TS) geometry to the reactant and product minima on the potential energy surface (PES) in mass-weighted Cartesian coordinates. An option to calculate the IRC has been implemented in many quantum chemical program packages and utilized in many applications. Recent developments in the IRC approach can be found in the literature.[3]

The IRC calculation requires the location of the TS geometry beforehand. The TS geometry corresponds to a first-order saddle point on the PES, and thus, TS geometry optimization has been more challenging than the geometry optimization of the minima. A number of TS optimization methods have ever been proposed.[4] Double-ended methods such as the nudged elastic band (NEB) method[5] require a pair of reactant and product geometries to locate TS, while there are several single-ended constrained optimization methods which require only reactant geometry. In the distinguished coordinate or coordinate driving methods,[6-10] one coordinate is chosen to drive the reactant into the product, and constraint optimization is performed with the selected coordinate fixed, resulting in the energy profile for the reaction process. The gradient extremals following (GEF) method searches TS by following stationary points of gradient norm on iso-potential surface.[11-21] The reduced gradient following (RGF) method[22-26] and the Newton trajectories (NTs)[27-31] are related to the distinguished coordinate method which requires choosing a coordinate. RGF and NTs, however, continuously trace the curve on which stationary (not necessarily minimum) condition of energy holds,

except for the selected direction. This procedure allows RGF and NTs to improve the problems[8-10] of the distinguished coordinate method.[22]

The anharmonic downward distortion (ADDF) method[32,33] is also one of the constrained optimization methods. In the ADDF method, the normal coordinates are scaled by square root of their corresponding eigenvalues for a given equilibrium structure (EQ). ADDF basically steps in the radial direction of the hypersphere centered at the EQ and minimizes energy on the hypersphere; non-minimum points are additionally traced in practice.[33] Similar to the distinguished coordinate method, ADDF uses a predictor-corrector procedure, but it does not require choosing any direction because the step direction at every step is uniquely determined as the radial direction of the hypersphere.

The ADDF method has shown its efficiency in many applications.[34-38] Very recently, Mitsuta and coworkers formulated a methodology to determine the reaction path network on a free energy surface using the ADDF concept.[39,40] However, only a few papers empirically argue the behavior of the ADDF path.[32,33] This is in contrast to the cases of GEF[17,20,21] and RGF (or NTs).[23,24] To better understand the performance of ADDF, the mathematical aspects of the ADDF path need to be examined in detail.

In this paper, we attempt to grasp the geometrical feature of the ADDF path by mathematical analysis. We first show that the number of the ADD stationary paths (= traces of the ADD stationary points on a hypersphere) intersecting the potential minimum is strictly determined by the third-order terms of the Taylor expansion of the PES at minimum; as an example, the ADD stationary paths are determined for the H_2O molecule. Next, we confirm that the overlooking of TSs by the ADDF method is caused essentially by the bifurcation feature of the ADD stationary paths. Though overlooking of TSs by the ADDF method was already discussed from empirical viewpoint,[33,36] the relation between overlooking TSs and bifurcation has not been discussed from mathematical viewpoint. Third, we discuss the approach to tracking the ADD inflection point in addition to the ADD maximum point in the ADDF method. Finally, we discuss the completeness of the ADDF method to explore all the TS geometries from the potential minimum.

ADDF Method

The geometrical structure of an N -atomic molecule is specified with vector $\boldsymbol{x} = (\boldsymbol{x}_1, \ldots, \boldsymbol{x}_N)$, where $\boldsymbol{x}_i = (x_{i1}, x_{i2}, x_{i3})$ denotes the *i*th nuclear Cartesian coordinates. The mass-weighted coordinates are defined by $\boldsymbol{q} = \boldsymbol{M}^{1/2}\boldsymbol{x}$ in which the *ij*th element of $\boldsymbol{M}$ is given by $M_{ij} = m_{\left[\frac{i+2}{3}\right]}\delta_{ij}$, where m_k is the kth nuclear mass and symbols $[\,]$ and δ_{ij} are Gauss symbol and Kronecker delta, respectively. In mass-weighted coordinates, differential operator $\nabla = \left(\frac{\partial}{\partial \boldsymbol{x}_1}, \ldots, \frac{\partial}{\partial \boldsymbol{x}_N}\right)$ is transformed into $\boldsymbol{M}^{-1/2}\nabla$, and the Hessian matrix is given by $\boldsymbol{M}^{-1/2}\nabla\nabla V(\boldsymbol{x})\boldsymbol{M}^{-1/2}$, where $V(\boldsymbol{x})$ is potential energy at $\boldsymbol{x}$. The normal mode vectors, $\{\boldsymbol{L}_i\ (i = 1, \ldots, f)\}$, are the normalized eigenvectors of the mass-weighted Hessian matrix with nonzero eigenvalues, $\{\lambda_i\ (i = 1, \ldots, f)\}$, which correspond to force constants. Hence, f denotes the degree of freedom of the system ($f = 3N - 6$).

The ADD function around the EQ, V_{ADD}, is defined by

$$V_{\mathrm{ADD}}(\boldsymbol{Q}) = \frac{1}{2}\sum_{i=1}^{f}\lambda_i Q_i^2 - V(\boldsymbol{Q}), \qquad (1)$$

where $\boldsymbol{Q} = \sum_{i=1}^{f} Q_i\,\boldsymbol{L}_i$ are normal coordinates and V at the EQ is set to be zero ($V(\boldsymbol{0}) = 0$). V_{ADD} is the difference between the harmonic potential energy and real potential energy and is schematically illustrated in Fig. 1. By introducing the scaled normal coordinates,

$$\bar{Q}_i = \sqrt{\lambda_i}Q_i\ (i = 1, \ldots, f), \qquad (2)$$

V_{ADD} on a hypersphere $S(R)$ of radius R centered at the origin is rewritten as follows:

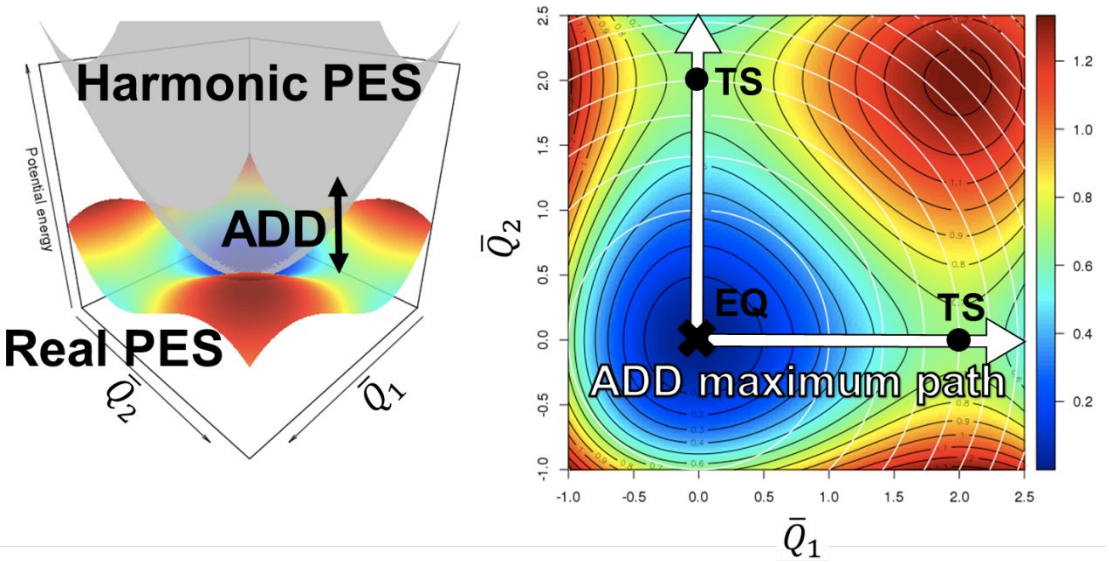

Figure 1. Schematic of ADD and ADD maximum path. Left panel: Harmonic PES and real PES around the EQ are shown as the transparent surface and iridescent surface, respectively. Right panel: Two-dimensional map of the real PES in the left panel. Black lines and white lines are contours of the real PES and the harmonic PES, respectively. The ADD maximum path follows ADD maximum points (= minimum energy points) on the circles centered at the EQ, shown by white arrows from the EQ.

$$V_{\mathrm{ADD}}(\bar{\boldsymbol{Q}}) = \frac{R^2}{2} - V(\bar{\boldsymbol{Q}}), \qquad (3)$$

where $R^2 = \sum_{i=1}^{f} \bar{Q}_i^2$. Then, the local maxima of V_{ADD} on $S(R)$ are equivalent to the local minima of the real potential energy on $S(R)$.

Here, we briefly explain the procedure of the ADDF method.

STEP 1. Let i be equal to 0. Search all the ADD maxima on hypersphere S_i of radius $R_i(>0)$ centered at the origin (EQ). Let $\bar{\boldsymbol{Q}}^{i,k}$ be the *k*-th ADD maximum point on S_i.

STEP 2. Let i increase by one. Project $\bar{\boldsymbol{Q}}^{i-1,k}$ onto a new hypersphere S_i of radius R_i $(> R_{i-1})$. Then, search the local ADD maxima from the projected points.

STEP 3. If the energy at $\bar{\boldsymbol{Q}}^{i,k}$ is higher than that at $\bar{\boldsymbol{Q}}^{i-1,k}$, return to STEP 2. Otherwise, go to STEP 4.

STEP 4. Search the TS geometry from $\bar{\boldsymbol{Q}}^{i,k}$.

Following the above procedure, one can locate the TS geometries connected to the EQ. The initial radius R_0 is determined so that the displacement along the normal mode with the largest force constant becomes 0.03 Å, while the radius of the ith hypersphere is given by $R_i = i^2\varepsilon$, where ε (= R_1) is determined so that the displacement along the normal mode with the largest force constant becomes 0.1 Å.[36] In the ADDF method implemented in the GRRM14 program,[41] the search for the local minima on the initial hypersphere (in STEP 1) is conducted by the iterative optimization and elimination (IOE) method.[33] The procedure of the IOE method on the initial hypersphere is as follows:

STEP A. Locate the ADD maxima on the initial hypersphere S_0 starting from $2f$ points at the intersections of S_0 with the respective normal coordinate directions. Let the located maxima denoted by $\bar{\boldsymbol{Q}}^{0,1}, \ldots, \bar{\boldsymbol{Q}}^{0,m}$.

STEP B. Eliminate the located ADD maxima by adding the shape functions $G_1(\bar{\boldsymbol{Q}}^{0,1}), \ldots,$

$G_m(\overline{\boldsymbol{Q}}^{0,m})$ to potential energy V. Let the potential energy after the elimination denoted by V_a $(a = m)$.

STEP C. Locate another ADD maximum of V_a on S_0 and let the located maximum denoted by $\overline{\boldsymbol{Q}}^{0,a+1}$.

STEP D. Eliminate the located ADD maximum by adding shape function $G_{a+1}(\overline{\boldsymbol{Q}}^{0,a+1})$ to V_a, and let the potential energy after the elimination denoted by V_{a+1}. Let a increase by 1 and return to **STEP C**.

STEP C and STEP D are repeated until no new ADD maximum point with ADD larger than a given threshold is found anymore. The IOE attempts to find all the ADD maximum points on the initial hypersphere. Additionally, the IOE method is expected to reveal the ADD maxima hidden by other large ADD maxima.[33] Here, it must be emphasized that the ADDF method traces not only ADD maximum points but also ADD non-maximum points. Except for the ADD maxima located at STEP A, located points are not necessarily ADD maximum points on the original potential V due to the added shape functions. If the ratio of ADD to the amplitude of shape function at a located point is smaller than threshold, the point is discarded and not traced anymore.[33] As far as the ratio is larger than the threshold, any located point will be traced even if it is not close to any ADD maximum points on the original potential. While this seems wasteful, it has a merit for global reaction path search because trace of such artificial maximum points sometimes leads to new ADD maximum points.[33] Except for the initial hypersphere, a computation of ADD maxima on a hypersphere is conducted by the predictor-corrector IOE (PC-IOE) method,[33] in which the ADD maxima on the last hypersphere are projected onto the current hypersphere, and then, STEP A is conducted starting from the projected points. A computation of the ADD maximum point and elimination of the maximum are performed in a descending order of the magnitude of the ADD on the last hypersphere.

As described above, the ADDF method follows not only the ADD maximum points but also some additional points. The paths followed by the ADDF method are called ADDF paths. Because the behavior of ADDF paths depends on the form of the shape function, we first analyze the behavior of ADD maximum paths. Then, we compare the ADD maximum paths and the ADDF paths, taking the case of a H_2O molecule as an example.

Maximum Number of ADD Stationary Paths Intersecting EQ

The ADD maximum path traces the ADD maximum point on $S(R)$ by sequentially expanding radius R. The ADD maxima on $S(R)$ can be located by the Lagrange multiplier method. First, we introduce the following function,

$$\Phi(\overline{\boldsymbol{Q}}, \mu) = V_{\mathrm{ADD}}(\overline{\boldsymbol{Q}}) - \frac{\mu}{2}\left(\sum_{i=1}^{f} \bar{Q}_i^2 - R^2\right). \quad (4)$$

If $\overline{\boldsymbol{Q}}$ corresponds to a stationary point of V_{ADD} on $S(R)$, the following equations hold:

$$\frac{\partial}{\partial \bar{Q}_i}\Phi(\overline{\boldsymbol{Q}}, \mu) = 0 \quad (i = 1, \ldots, f), \quad (5)$$

$$\frac{\partial}{\partial \mu}\Phi(\overline{\boldsymbol{Q}}, \mu) = 0. \quad (6)$$

The stationary points can be classified into maximum, minimum, and saddle points based on the Hessian matrix of potential energy on the hypersphere. The solutions of Eqs. (5) and (6) are called the ADD stationary path in this paper.

To understand the law that determines the number of the ADD stationary paths that intersects the EQ, the behavior of the ADD stationary paths near the EQ should be analyzed. Since Eqs. (5) and (6) must hold identically along the ADD stationary paths, the derivatives of the left-hand sides of Eqs. (5) and (6) are also zero along the ADD stationary paths. Generally,

$$d^r \frac{\partial}{\partial \bar{Q}_i} \Phi(\bar{\boldsymbol{Q}}, \mu) = 0 \quad (i = 1, \ldots, f), \tag{7}$$

$$d^r \frac{\partial}{\partial \mu} \Phi(\bar{\boldsymbol{Q}}, \mu) = 0, \tag{8}$$

hold along the ADD stationary paths for any nonnegative integer r. Eqs. (7) and (8) may be considered as r-th order perturbation equation, with the radius of hypersphere being the perturbation parameter. When $r = 1$, Eqs. (7) and (8) can be written as follows:

$$\sum_{j=1}^{f} \frac{\partial^2 V_{\mathrm{ADD}}(\bar{\boldsymbol{Q}})}{\partial \bar{Q}_i \partial \bar{Q}_j} d\bar{Q}_j - \bar{Q}_i d\mu - \mu d\bar{Q}_i = 0 \quad (i = 1, \ldots, f), \tag{9}$$

$$\sum_{i=1}^{f} \bar{Q}_i d\bar{Q}_i - R dR = 0. \tag{10}$$

At the EQ, Eq. (10) clearly holds. Since V_{ADD} does not include monomials of $\bar{Q}_i$s with a total degree lower than 3 (see Eq. (1)), $\frac{\partial^2 V_{\mathrm{ADD}}(\mathbf{0})}{\partial \bar{Q}_i \partial \bar{Q}_j} = 0$. Thus, at the EQ,

$$\mu = 0 \tag{11}$$

holds. Note that if V_{ADD} included quadratic term, Eq. (9) gives a linear eigenvalue equation. However, because there is no quadratic term in V_{ADD}, the problem becomes nonlinear as shown below. When $r = 2$, Eqs. (7) and (8) can be written as follows:

$$\sum_{j=1}^{f} \sum_{k=1}^{f} \frac{\partial^3 V_{\mathrm{ADD}}(\bar{\boldsymbol{Q}})}{\partial \bar{Q}_i \partial \bar{Q}_j \partial \bar{Q}_k} d\bar{Q}_j d\bar{Q}_k - 2 d\bar{Q}_i d\mu + \sum_{j=1}^{f} \frac{\partial^2 V_{\mathrm{ADD}}(\bar{\boldsymbol{Q}})}{\partial \bar{Q}_i \partial \bar{Q}_j} d^2\bar{Q}_j - \bar{Q}_i d^2\mu - \mu d^2\bar{Q}_i = 0 \quad (i = 1, \ldots, f), \tag{12}$$

$$\sum_{i=1}^{f} (d\bar{Q}_i)^2 - (dR)^2 + \sum_{i=1}^{f} \bar{Q}_i d^2\bar{Q}_i - R d^2 R = 0. \tag{13}$$

Using Eq. (11), $\frac{\partial^2 V_{\mathrm{ADD}}(\mathbf{0})}{\partial \bar{Q}_i \partial \bar{Q}_j} = 0$, and $\frac{\partial^3 V_{\mathrm{ADD}}(\bar{\boldsymbol{Q}})}{\partial \bar{Q}_i \partial \bar{Q}_j \partial \bar{Q}_k} = -\frac{\partial^3 V(\bar{\boldsymbol{Q}})}{\partial \bar{Q}_i \partial \bar{Q}_j \partial \bar{Q}_k}$, Eqs. (12) and (13) can be written as follows:

$$-\sum_{j=1}^{f} \sum_{k=1}^{f} \frac{\partial^3 V(\mathbf{0})}{\partial \bar{Q}_i \partial \bar{Q}_j \partial \bar{Q}_k} d\bar{Q}_j d\bar{Q}_k - 2 d\bar{Q}_i d\mu = 0 \quad (i = 1, \ldots, f), \tag{14}$$

$$\sum_{i=1}^{f} (d\bar{Q}_i)^2 - (dR)^2 = 0. \tag{15}$$

Eqs. (14) and (15) can be regarded as $f + 1$ homogeneous polynomial equations with variables $d\bar{Q}_1, \ldots, d\bar{Q}_f, d\mu$, and dR. Thus, the ratio of these variables can be obtained by solving Eqs. (14) and (15). Since the absolute values of these infinitesimal variables are trivial, we identify $(cd\bar{Q}_1, \ldots, cd\bar{Q}_f, cd\mu, cdR)$ with $(d\bar{Q}_1, \ldots, d\bar{Q}_f, d\mu, dR)$, where c is an arbitrary nonzero complex number, and regard the ratio as a root of Eqs. (14) and (15). The independent real roots of Eqs. (14) and (15) correspond to the directions of the ADD stationary paths intersecting the EQ. One can see that Eqs. (5) and (6) with $V_{\mathrm{ADD}}(\bar{\boldsymbol{Q}})$ truncated at the third-order Taylor expansion are equivalent to Eqs. (14) and (15), respectively. Thus, the problem to determine the number of the ADD stationary paths intersecting the EQ is reduced to determine the number of stationary points of the third-order terms of the Taylor expansion of the ADD function around the EQ (denoted as $V_{\mathrm{ADD}}^{(3)}$ below) on a hypersphere with any radius other than zero. A three-dimensional version of this problem was solved by Kuznetsov and Kholshevnikov.[42] Ni, Qi, Wang, and Wang solved the problem in the case of an even degree,[43] and later, Cartwright and Sturmfels generalized the result to the case of an odd degree.[44] According to the work by Cartwright and Sturmfels, the

maximum number of stationary points of homogeneous polynomial of n variables with a degree of $m(\geq 3)$ on a hypersphere centered at the origin is given by $2\{(m-1)^n - 1\}/(m-2)$ when the number of the stationary point is finite. Thus, the possible maximum number of the ADD stationary paths intersecting the EQ (= the maximum number of real roots of Eq. (14)) is given by

$$2^{f+1} - 2. \qquad (16)$$

This number is not deterministic because of the nonlinearity of Eq. (14), and is larger than the number of the gradient extremal paths $2f$.[21]

As a demonstration, we carried out reaction path search calculations for H_2O.[45] Hence, we adopt an algebraic geometry method that is a partial modification of Auzinger's algorithm[46] to compute all common roots of multivariate polynomials by which all the ADD stationary points on this sphere could be computed noniteratively. The rank of saddle points does not affect the difficulty to locate them because Auzienger's algorithm computes stationary points as eigenvectors of a linear eigenvalue problem, which are easily obtained by various diagonalization codes. The electronic structure computations were carried out by the spin-restricted Hartree-Fock (RHF) method with a 6-31G(d,p) basis set using Gaussian09.[47] The PES around the EQ was approximated by the fourth-order Taylor expansion in terms of normal coordinates, where the second-, third-, and fourth-order derivatives were computed using an option of anharmonic frequency calculations implemented in Gaussian09. By using the scaled normal coordinates defined by Eq. (2), an isosurface of the harmonic potential becomes the sphere centered at the EQ. Figure 2 shows the ADD contour diagram of the H_2O molecule on a sphere of radius 0.3 hartree$^{1/2}$ viewed from six directions, where red indicates a large ADD and low-potential-energy region, while blue indicates a small ADD and high-potential-energy region. The number of the ADD stationary points on the sphere is 14, comprising four maxima (Max1-Max4), six saddle points (S1-S6), and four minima (Min1-Min4)). This number 14 is equal to the upper limit, $2^{f+1} - 2$ $(f = 3)$, calculated using Eq. (16).

Figure 3 shows the ADD stationary paths determined by tracing the ADD stationary points while increasing the sphere radius as (a) R = 0 to 1.0 hartree$^{1/2}$ and (b) R = 0 to 0.3 hartree$^{1/2}$. The number of ADD stationary points on the sphere varies with the sphere radius, as shown in Fig. 3a. One ADD saddle path (= a trail of ADD saddle points) changes into an ADD maximum path (path 5) with two new ADD saddle paths at a radius of 0.66 hartree$^{1/2}$ (called pitchfork bifurcation[23,48]). Because of the bifurcation, the number of ADD stationary paths increases to 20 on a sphere of radius 1.0 hartree$^{1/2}$. In the vicinity of the EQ, the opposite direction of each ADD maximum path corresponds to the ADD minimum path, and the opposite direction of each ADD saddle path corresponds to another ADD saddle path. This behavior is understood by the parity of $V_{\mathrm{ADD}}^{(3)}$. Since $V_{\mathrm{ADD}}^{(3)}$ is the third-order homogeneous polynomial, $V_{\mathrm{ADD}}^{(3)}(-d\bar{\boldsymbol{Q}}) = -V_{\mathrm{ADD}}^{(3)}(d\bar{\boldsymbol{Q}})$ holds and the opposite point of the ADD stationary point also corresponds to the ADD stationary point. Moreover, the opposite point of the l-th order ADD saddle point $(0 \leq l < f-1)$ corresponds to the $(f-1-l)$-th order ADD saddle point because the Hessian matrix of $V_{\mathrm{ADD}}^{(3)}$ on a sphere (see Eq. (21)) is also antisymmetric with respect to a spatial inversion. Figure 3c shows the other characteristic bifurcation in the case of H_2O, which are transcritical bifurcation and hysteresis loop.[48] At the transcritical bifurcation point, the ADD saddle path and the ADD minimum path intersect and the nature of the path is swapped. In the hysteresis loop, the ADD saddle path changes first into the ADD maximum path and then changes into the ADD saddle path again.

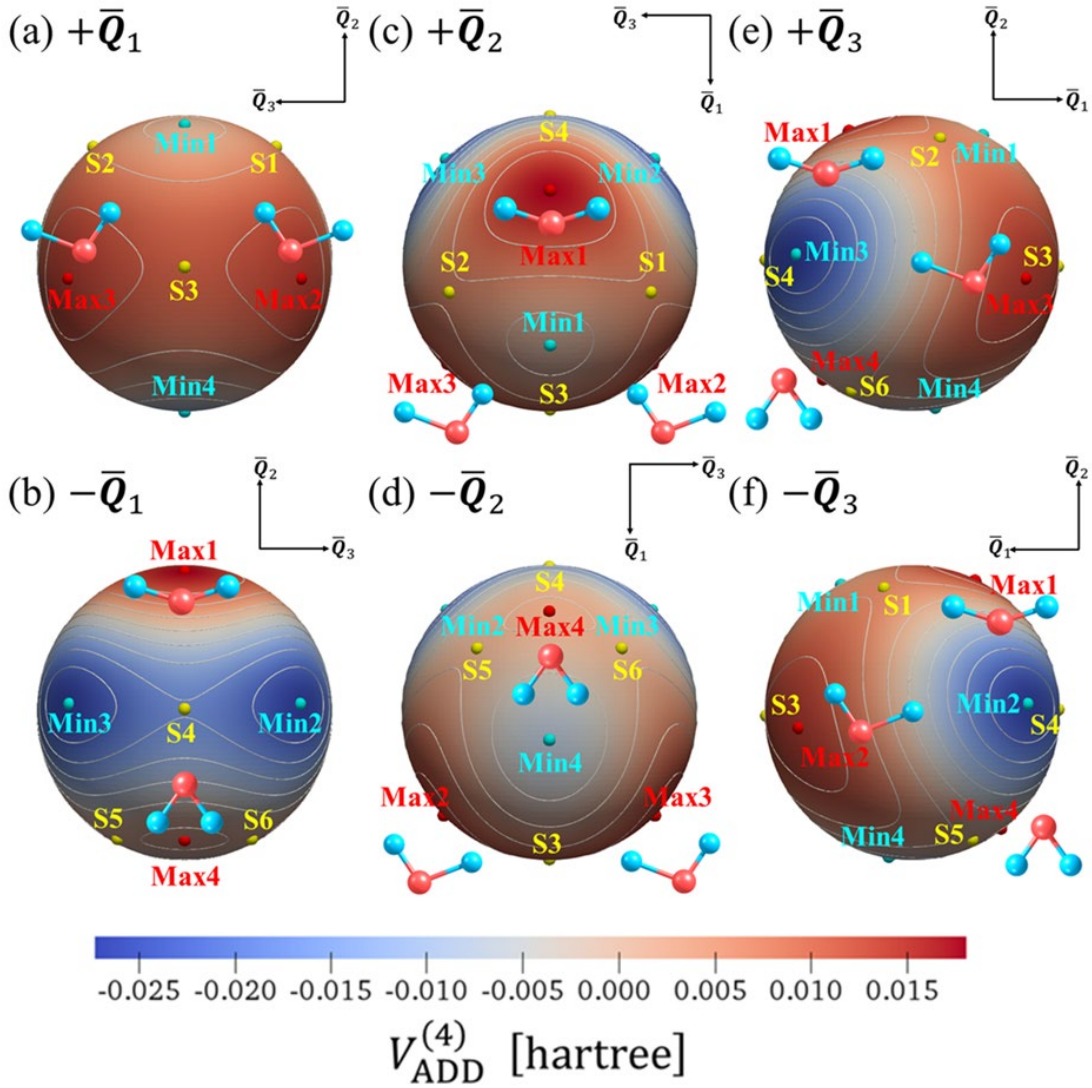

Figure 2. ADD contour diagram of the H_2O molecule on a sphere of radius 0.3 hartree$^{1/2}$ centered at the EQ. Each panel shows a bird's-eye view from the direction of (a) $+\bar{Q}_1$, (b) $-\bar{Q}_1$, (c) $+\bar{Q}_2$, (d) $-\bar{Q}_2$, (e) $+\bar{Q}_3$, and (f) $-\bar{Q}_3$, where $\bar{Q}_1$, $\bar{Q}_2$, and $\bar{Q}_3$ are scaled normal coordinates for OH symmetric stretching (A_1), H-O-H bending (A_1), and OH antisymmetric stretching (B_2) vibrational modes, respectively. The ADD function is approximated by the fourth-order polynomials (denoted as $V_{\mathrm{ADD}}^{(4)}$), where white lines are the contours of $V_{\mathrm{ADD}}^{(4)}$. The value of $V_{\mathrm{ADD}}^{(4)}$ is shown by color (blue ~ red), and the red points (Max1-Max4), yellow points (S1-S6), and cyan points (Min1-Min4) denote ADD maxima, ADD saddles, and ADD minima, respectively. Ball-stick models beside the ADD maxima show the corresponding H_2O geometries.

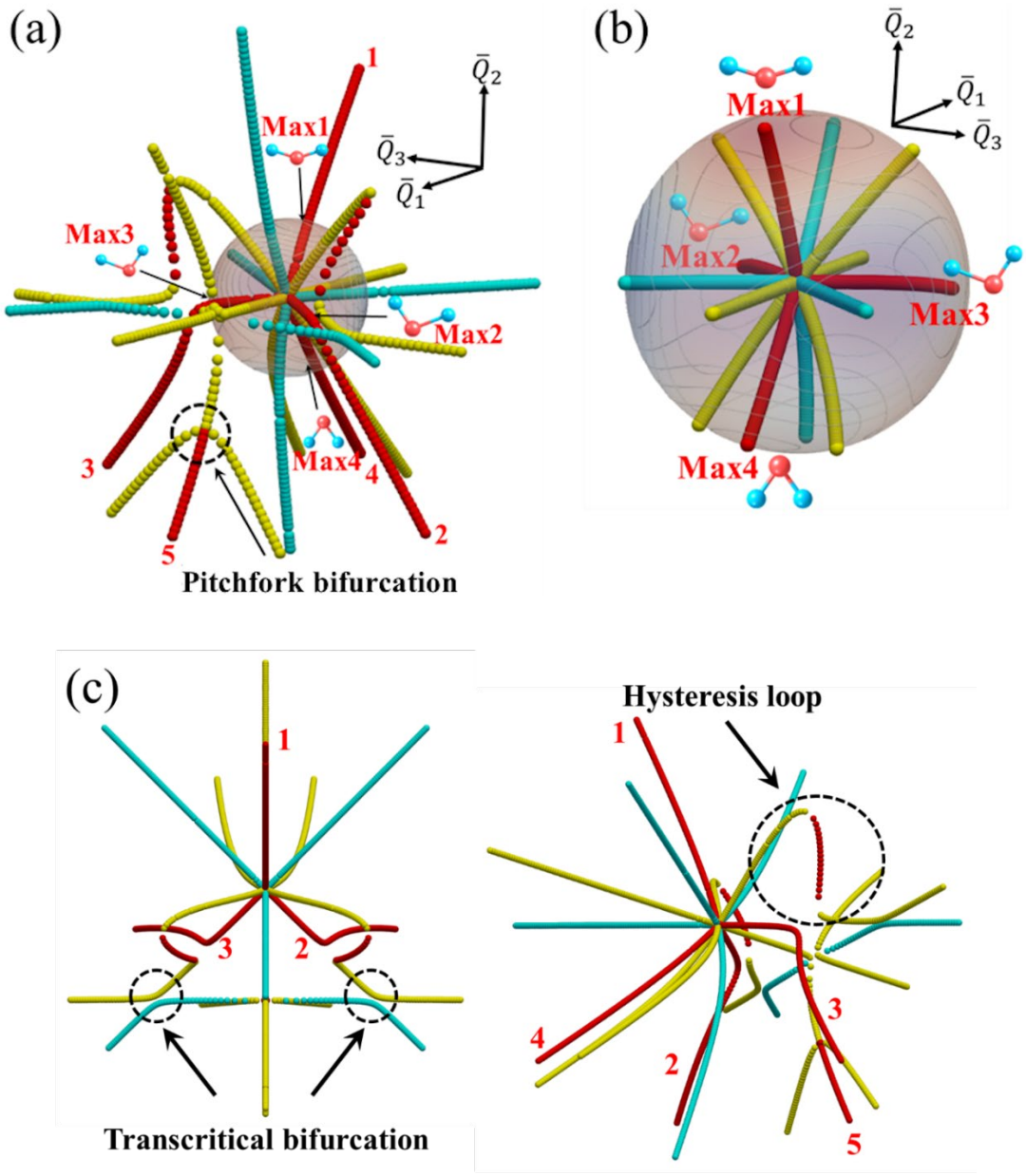

Figure 3. ADD stationary paths of H_2O determined by tracing the stationary points of $V_{\mathrm{ADD}}^{(4)}$ while increasing the sphere radius as (a) R = 0 to 1.0 hartree$^{1/2}$ and (b) R = 0 to 0.3 hartree$^{1/2}$. Red, yellow, and cyan points correspond to the ADD maxima, ADD saddle points, and ADD minima, respectively. The transparent sphere is the same as that shown in Fig. 2. In (a), pitchfork bifurcation of the ADD saddle path occurs at R = 0.66 hartree$^{1/2}$, resulting in one ADD maximum and two ADD saddle paths. The other characteristic bifurcation is shown in (c).

Bifurcation of ADD Stationary Path

As shown in the case of H_2O, the number of ADD maxima on the sphere may change due to the bifurcation of the ADD stationary paths. ADD maximum path 5 in Fig. 3a appears owing to pitchfork bifurcation at R = 0.66 hartree$^{1/2}$. To confirm that this bifurcation is not an artifact caused by an approximation to the PES, we also performed the ADD maximum path search for H_2O based on the real PES by the spin-unrestricted Hartree-Fock (UHF) method with 6-31G(d,p) basis sets, using our own ADD stationary path search program. The UHF method was employed with the option, Stable=Opt, in Gaussian09, to describe the dissociation pathway into two fragments of doublet spin multiplicity. The calculated ADD maximum paths are shown in the Supporting Information, which are basically the same as those obtained with the fourth-order Taylor expansion PES. It was shown that the pitchfork bifurcation point appears on a sphere of radius R = 0.78 hartree$^{1/2}$ on the real PES, and ADD maximum path 5 caused by bifurcation leads to TS in the dissociation to O + H_2.

We also performed the ADD maximum path search for H_2O based on the real PES by UHF/6-31G(d,p) using the GRRM14 program[41] with the options MO GUESS, Opt=Tight, and Stable=Opt. In the GRRM program, the IOE method was originally introduced to detect the direction of the hidden ADD maxima on the initial hypersphere,[32,33] but it does not always work as expected. Figure 4 shows the ADDF paths (shown by orange dots) computed by GRRM14.[41] Dots on the floor are projected points of the ADDF paths. Five ADDF paths were obtained, but one was discarded in the very early step of the ADDF procedure. Thus, only four ADDF paths are shown in Fig. 4, almost coinciding with the ADD maximum paths near the EQ. This means that the IOE method merely located the ADD maxima of the original PES, and the direction of the pitchfork bifurcation on the initial sphere (hidden ADD maximum) could not be detected. One ADDF path leads to the linear structure (H-O-H) of the second-order saddle point (SOSP), while two ADDF paths lead to the dissociation channels (DC) to OH + H.[49] The rest leads to X''' *via* geometries X, X', and X''. Around X, the ADD maximum turns into an ADD saddle. Without the IOE technique, the optimization on the next sphere converges to either of the two DCs. However, with the IOE technique, X' was located instead of a geometry on either of the DCs, because ADD maximum basins around DCs are blocked by the shape function.[50] Then, the ADD path continues till X'', but in the next sphere, it falls in the basin of the ADD maximum around X'''. At X''', the potential energy starts decreasing along the ADDF path. Then, the ADDF method is stopped, and TS(guess) is located as the energy-top point along the ADDF path. The TS optimization from TS(guess) led to TS1 (linear HH…O), which connects O + H_2 and OH + H. In fact, the TS obtained by the ADDF method is sensitive to any change in the step size when expanding the sphere radius. When ε is determined so that the displacement becomes 0.02 Å (the default is 0.1 Å), the located TS was not TS1 but TS2 that connects the EQ and O + H_2 keeping the C_{2v} symmetry. When the displacement was set to 0.09 Å, both structures were not found.

Ohno and Maeda discussed overlooking of the TSs in ADDF computations from empirical view.[33] They claimed that this is because small ADD is covered by large ADDs and cannot be detected by the IOE method due to its fitting error in shape functions.[33] In the H_2O case, the ADD in the direction of H_2 dissociation channel (via TS2) is small and covered by the large ADDs of H atom dissociation channels. This explanation is true, but overlooking of TSs can be understood more clearly in terms of bifurcation. It is important to understand the bifurcation of the ADD stationary path to determine whether the ADDF method is able to locate all TSs. In the following section, we derive the conditions necessary for the ADD stationary path to bifurcate and investigate the typical bifurcation pattern.

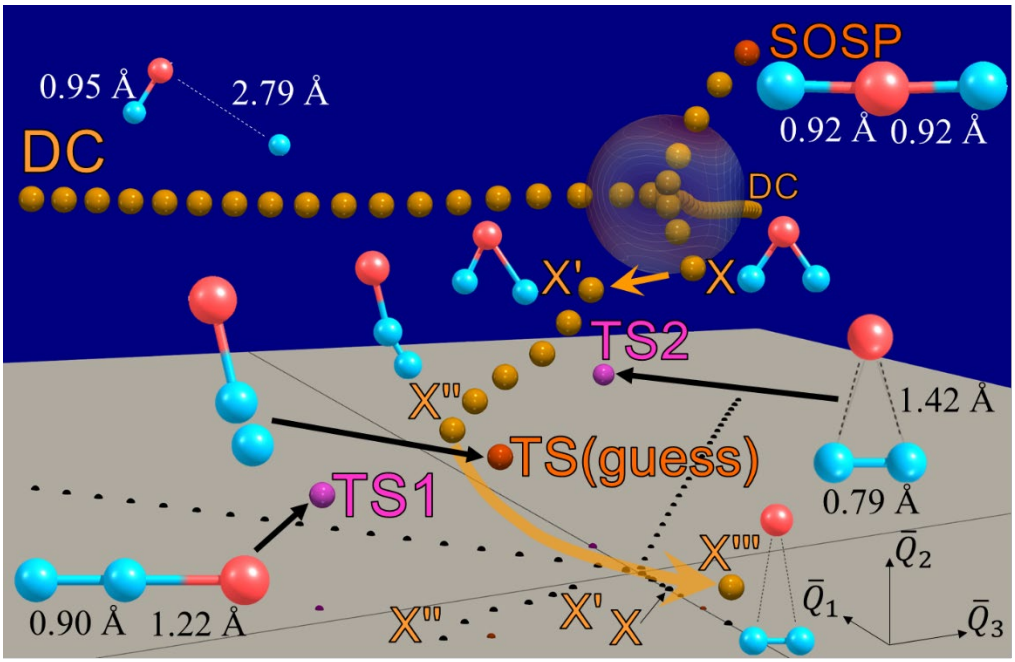

Figure 4. ADDF paths (orange dots) of the H_2O molecule computed by GRRM14. Dots on the floor are the projected points of ADDF paths and TS geometries, and the two orthogonal lines on the floor denote the $\bar{Q}_1$ and $\bar{Q}_3$ axes. The transparent sphere is the same as that shown in Fig. 2. Four ADDF paths were obtained: one leads to SOSP, two lead to DC to OH + H, and the remaining leads to X''' *via* geometries X, X', and X''. Starting from the TS(guess), the top of the ADDF path, the TS with the linear structure (TS1) was obtained, but the TS with the C_{2v} symmetry (TS2) was overlooked.

The necessary condition for the ADD stationary path to bifurcate is the singularity of the Hessian matrix of the ADD function on the hypersphere. First, we derive the Hessian matrix of the ADD function at a point on the hypersphere. Let the scalar product of two vectors $\boldsymbol{a}$ and $\boldsymbol{b}$ be denoted by $\langle \boldsymbol{a}, \boldsymbol{b} \rangle$ and $\bar{\boldsymbol{Q}}$ be a point on the hypersphere $S(R) = \{\bar{\boldsymbol{Q}} | \langle \bar{\boldsymbol{Q}}, \bar{\boldsymbol{Q}} \rangle = R^2, R \in (0, \infty)\}$. There are $f-1$ orthonormal vectors $\boldsymbol{e}_1(\bar{\boldsymbol{Q}}), \ldots, \boldsymbol{e}_{f-1}(\bar{\boldsymbol{Q}})$ tangent to $S(R)$ and one outward normal vector $\boldsymbol{n}(\bar{\boldsymbol{Q}})$. On the hypersphere $S(R)$, $\boldsymbol{n}(\bar{\boldsymbol{Q}}) = \bar{\boldsymbol{Q}}/\sqrt{\langle \bar{\boldsymbol{Q}}, \bar{\boldsymbol{Q}} \rangle}$ holds. We omit the dependent variables of $\boldsymbol{e}_1(\bar{\boldsymbol{Q}}), \ldots, \boldsymbol{e}_{f-1}(\bar{\boldsymbol{Q}})$ and $\boldsymbol{n}(\bar{\boldsymbol{Q}})$ in the discussion below. The Hessian matrix of the ADD function $V_{\mathrm{ADD}}(\bar{\boldsymbol{Q}})$ is given by

$$\langle \boldsymbol{e}_\mu, \frac{\partial}{\partial \bar{\boldsymbol{Q}}} \rangle \langle \boldsymbol{e}_\nu, \frac{\partial}{\partial \bar{\boldsymbol{Q}}} \rangle V_{\mathrm{ADD}}$$
$$= \langle \boldsymbol{e}_\mu, \langle \boldsymbol{e}_\nu, \frac{\partial}{\partial \bar{\boldsymbol{Q}}} \rangle \frac{\partial}{\partial \bar{\boldsymbol{Q}}} \rangle V_{\mathrm{ADD}}$$
$$+ \langle \langle \boldsymbol{e}_\mu, \frac{\partial}{\partial \bar{\boldsymbol{Q}}} \rangle \boldsymbol{e}_\nu, \frac{\partial}{\partial \bar{\boldsymbol{Q}}} \rangle V_{\mathrm{ADD}}$$
$$(\mu, \nu = 1, \ldots, f-1). \qquad (17)$$

Here, $\langle \boldsymbol{e}_\mu, \frac{\partial}{\partial \bar{\boldsymbol{Q}}} \rangle \boldsymbol{e}_\nu$ in the f dimensional Euclidean space $\mathbb{R}^f$ can be written as the linear combination of $\boldsymbol{e}_1, \ldots, \boldsymbol{e}_{f-1}$ and $\boldsymbol{n}$:

$$\langle \boldsymbol{e}_\mu, \frac{\partial}{\partial \bar{\boldsymbol{Q}}} \rangle \boldsymbol{e}_\nu = \sum_{\lambda=1}^{f-1} \begin{Bmatrix} \lambda \\ \mu\nu \end{Bmatrix} \boldsymbol{e}_\lambda + \Omega_{\mu\nu} \boldsymbol{n}, \qquad (18)$$

where $\begin{Bmatrix} \lambda \\ \mu\nu \end{Bmatrix}$ and $\Omega_{\mu\nu}$ are the Christoffel symbols and the Euler-Schouten tensor, respectively. According to Riemannian geometry, by choosing

$\boldsymbol{e}_1, \ldots, \boldsymbol{e}_{f-1}$ as the basis of a geodesic coordinate system at $\overline{\boldsymbol{Q}}$,

$$\begin{Bmatrix} \lambda \\ \mu\nu \end{Bmatrix} = 0 \tag{19}$$

holds.[51] The Euler-Schouten tensor of the hypersphere is given by

$$\begin{aligned}
&\Omega_{\mu\nu} \\
&= \langle \boldsymbol{n}, \langle \boldsymbol{e}_\mu, \frac{\partial}{\partial \overline{\boldsymbol{Q}}} \rangle \boldsymbol{e}_\nu \rangle \\
&= -\langle \langle \boldsymbol{e}_\mu, \frac{\partial}{\partial \overline{\boldsymbol{Q}}} \rangle \boldsymbol{n}, \boldsymbol{e}_\nu \rangle \quad (\because \langle \boldsymbol{n}, \boldsymbol{e}_\nu \rangle = 0) \\
&= -\langle \langle \boldsymbol{e}_\mu, \frac{\partial}{\partial \overline{\boldsymbol{Q}}} \rangle \frac{\overline{\boldsymbol{Q}}}{\sqrt{(\overline{\boldsymbol{Q}}, \overline{\boldsymbol{Q}})}}, \boldsymbol{e}_\nu \rangle \quad \left(\because \boldsymbol{n} = \frac{\overline{\boldsymbol{Q}}}{\sqrt{\langle \overline{\boldsymbol{Q}}, \overline{\boldsymbol{Q}} \rangle}} \right) \\
&= -\langle \frac{1}{\sqrt{\langle \overline{\boldsymbol{Q}}, \overline{\boldsymbol{Q}} \rangle}} \boldsymbol{e}_\mu - \frac{\langle \boldsymbol{e}_\mu, \overline{\boldsymbol{Q}} \rangle}{\langle \overline{\boldsymbol{Q}}, \overline{\boldsymbol{Q}} \rangle} \boldsymbol{n}, \boldsymbol{e}_\nu \rangle \\
&= -\frac{\delta_{\mu\nu}}{R}.
\end{aligned} \tag{20}$$

Thus, using Eqs. (18), (19), and (20), Eq. (17) is rewritten as

$$\begin{aligned}
&\langle \boldsymbol{e}_\mu, \frac{\partial}{\partial \overline{\boldsymbol{Q}}} \rangle \langle \boldsymbol{e}_\nu, \frac{\partial}{\partial \overline{\boldsymbol{Q}}} \rangle V_{\mathrm{ADD}} \\
&= \langle \boldsymbol{e}_\mu, \langle \boldsymbol{e}_\nu, \frac{\partial}{\partial \overline{\boldsymbol{Q}}} \rangle \frac{\partial}{\partial \overline{\boldsymbol{Q}}} \rangle V_{\mathrm{ADD}} \\
&\quad - \frac{\delta_{\mu\nu}}{R} \langle \boldsymbol{n}, \frac{\partial}{\partial \overline{\boldsymbol{Q}}} \rangle V_{\mathrm{ADD}}.
\end{aligned} \tag{21}$$

Eq. (21) is the Hessian matrix of the ADD function on $S(R)$. The first term is the Hessian matrix of the ADD function on the hyperplane tangent to $S(R)$. The second term originates from the curvature of $S(R)$. Note that the Hessian matrix of the ADD function on $S(R)$ is not equal to that on the hyperplane normal to the ADD stationary path.

Next, we derive the necessary conditions for the ADD stationary path to bifurcate. Bifurcation of the ADD stationary path occurs where its tangent vector is either tangent to the hypersphere or is not uniquely determined. Let $\overline{\boldsymbol{Q}}$ be an ADD stationary point so that $\langle \boldsymbol{e}_\mu, \frac{\partial}{\partial \overline{\boldsymbol{Q}}} \rangle V_{\mathrm{ADD}} = 0$ $(\mu = 1, \ldots, f-1)$ at $\overline{\boldsymbol{Q}}$. Since these equations hold identically on the ADD stationary path, their derivatives also hold along the ADD stationary path. The first-order derivative along the ADD stationary path is given by

$$\begin{aligned}
&d\left(\langle \boldsymbol{e}_\mu, \frac{\partial}{\partial \overline{\boldsymbol{Q}}} \rangle V_{\mathrm{ADD}} \right) \\
&= \langle d\overline{\boldsymbol{Q}}, \frac{\partial}{\partial \overline{\boldsymbol{Q}}} \rangle \left(\langle \boldsymbol{e}_\mu, \frac{\partial}{\partial \overline{\boldsymbol{Q}}} \rangle V_{\mathrm{ADD}} \right) \\
&\quad = 0 \quad (\mu = 1, \ldots, f-1).
\end{aligned} \tag{22}$$

The infinitesimal displacement $d\overline{\boldsymbol{Q}}$ is tangent to the ADD stationary path. Since $d\overline{\boldsymbol{Q}}$ is an f-dimensional vector, it can be written as the linear combination of $\boldsymbol{e}_1, \ldots, \boldsymbol{e}_{f-1}, \boldsymbol{n}$:

$$d\overline{\boldsymbol{Q}} = \sum_{\nu=1}^{f-1} \langle \boldsymbol{e}_\nu, d\overline{\boldsymbol{Q}} \rangle \boldsymbol{e}_\nu + \langle \boldsymbol{n}, d\overline{\boldsymbol{Q}} \rangle \boldsymbol{n}. \tag{23}$$

By substituting Eq. (23) into Eq. (22),

$$\begin{aligned}
&\sum_{\nu=1}^{f-1} \langle \boldsymbol{e}_\nu, d\overline{\boldsymbol{Q}} \rangle \langle \boldsymbol{e}_\nu, \frac{\partial}{\partial \overline{\boldsymbol{Q}}} \rangle \langle \boldsymbol{e}_\mu, \frac{\partial}{\partial \overline{\boldsymbol{Q}}} \rangle V_{\mathrm{ADD}} \\
&+ \langle \boldsymbol{n}, d\overline{\boldsymbol{Q}} \rangle \langle \boldsymbol{n}, \frac{\partial}{\partial \overline{\boldsymbol{Q}}} \rangle \langle \boldsymbol{e}_\mu, \frac{\partial}{\partial \overline{\boldsymbol{Q}}} \rangle V_{\mathrm{ADD}} \\
&\quad = 0 \quad (\mu = 1, \ldots, f-1)
\end{aligned} \tag{24}$$

We introduce $Hess$, $\boldsymbol{b}$, and A with the components shown below:

$$\begin{aligned}
Hess_{\mu\nu} &= \langle \boldsymbol{e}_\nu, \frac{\partial}{\partial \overline{\boldsymbol{Q}}} \rangle \langle \boldsymbol{e}_\mu, \frac{\partial}{\partial \overline{\boldsymbol{Q}}} \rangle V_{\mathrm{ADD}} \\
&\quad (\mu, \nu = 1, \ldots, f-1),
\end{aligned} \tag{25}$$

$$\begin{aligned}
b_\mu &= \langle \boldsymbol{n}, \frac{\partial}{\partial \overline{\boldsymbol{Q}}} \rangle \langle \boldsymbol{e}_\mu, \frac{\partial}{\partial \overline{\boldsymbol{Q}}} \rangle V_{\mathrm{ADD}} \\
&\quad (\mu = 1, \ldots, f-1),
\end{aligned} \tag{26}$$

$$\begin{aligned}
A_{\mu\nu} &= \begin{cases} Hess_{\mu\nu} & (\nu = 1, \ldots, f-1) \\ b_\mu & (\nu = f) \end{cases} \\
&\quad (\mu = 1, \ldots, f-1).
\end{aligned} \tag{27}$$

Then, Eq. (24) can be rewritten as

$$A d\overline{\boldsymbol{Q}} = \boldsymbol{0}. \tag{28}$$

In particular, by choosing the orthonormalized eigenvectors of $Hess$, $\boldsymbol{l}_1(\overline{\boldsymbol{Q}}), \ldots, \boldsymbol{l}_{f-1}(\overline{\boldsymbol{Q}})$, as the basis, Eqs. (25)–(27) are written as

$$Hess_{\mu\nu} = h_\mu \delta_{\mu\nu} \quad (\mu, \nu = 1, \ldots, f-1), \tag{29}$$

$$b_\mu = \langle \boldsymbol{n}, \frac{\partial}{\partial \overline{\boldsymbol{Q}}} \rangle \langle \boldsymbol{l}_\mu, \frac{\partial}{\partial \overline{\boldsymbol{Q}}} \rangle V_{\mathrm{ADD}} \quad (\mu = 1, \ldots, f-1), \tag{30}$$

$$A_{\mu\nu} = \begin{cases} h_\mu \delta_{\mu\nu} & (\nu = 1, \ldots, f-1) \\ b_\mu & (\nu = f) \end{cases} \quad (\mu = 1, \ldots, f-1), \tag{31}$$

and Eq. (28) is written as

$$h_\mu \langle \boldsymbol{l}_\mu, d\overline{\boldsymbol{Q}} \rangle = -b_\mu \langle \boldsymbol{n}, d\overline{\boldsymbol{Q}} \rangle \quad (\mu = 1, \ldots, f-1). \tag{32}$$

Eq. (32) is a set of $f-1$ linear equations with f variables, $\langle \boldsymbol{l}_1, d\overline{\boldsymbol{Q}} \rangle, \ldots, \langle \boldsymbol{l}_{f-1}, d\overline{\boldsymbol{Q}} \rangle, \langle \boldsymbol{n}, d\overline{\boldsymbol{Q}} \rangle$. The nontrivial solution of Eq. (32) is the tangent vector of an ADD stationary path, and it is classified into four cases. In the first case, the solution of Eq. (32) is unique and there is no bifurcation. In the second case, the solution is unique and the tangent vector of the ADD stationary path is also tangent to the hypersphere. In spite of the uniqueness of the solution, there is a possibility of bifurcation in this case. In the third case, there are some solutions. If there are more than one real solution, the stationary paths intersect. In the fourth case, there are some solutions and all the tangent vector of the stationary paths are also tangent to the hypersphere. These four cases are shown in detail as follows.

(CASE 1) No bifurcation: $h_\mu \neq 0$ $(\mu = 1, \ldots, f-1)$:

In this case, the solution of Eq. (32) is determined uniquely and given by

$$\begin{cases} \langle \boldsymbol{l}_\mu, d\overline{\boldsymbol{Q}} \rangle = -c \dfrac{b_\mu}{h_\mu} & (\mu = 1, \ldots, f-1) \\ \langle \boldsymbol{n}, d\overline{\boldsymbol{Q}} \rangle = c \end{cases}, \tag{33}$$

where c is an arbitrary constant. Thus, there is only one ADD stationary path with its tangent vector given by Eq. (33), which intersects point $\overline{\boldsymbol{Q}}$. If the sign of $\langle \boldsymbol{n}, d\overline{\boldsymbol{Q}} \rangle$ is positive, the radius of the hypersphere increases in the direction of $d\overline{\boldsymbol{Q}}$ and decreases in the direction of $-d\overline{\boldsymbol{Q}}$. Since the ADDF method follows the ADD maximum paths with the expansion of the hypersphere radius, the ADD maximum path is followed in the direction of $d\overline{\boldsymbol{Q}}$. Thus, the direction of the ADD stationary path to be followed is unique in this case, i.e., there is no bifurcation.

(CASE 2) Bifurcations without crossing of paths: $h_1 = 0$, $h_\mu \neq 0$ $(\mu = 2, \ldots, f-1)$ and $b_1 \neq 0$

In this case, the solution of Eq. (32) is determined uniquely and given by

$$\begin{cases} \langle \boldsymbol{l}_\mu, d\overline{\boldsymbol{Q}} \rangle = c\delta_{\mu 1} & (\mu = 1, \ldots, f-1) \\ \langle \boldsymbol{n}, d\overline{\boldsymbol{Q}} \rangle = 0 \end{cases}, \tag{34}$$

where c is an arbitrary constant. Although the solution is determined uniquely, there is a possibility of bifurcation in this case. The tangent vector of the ADD stationary path at $\overline{\boldsymbol{Q}}$ given by Eq. (34), $d\overline{\boldsymbol{Q}}$, is also tangent to the hypersphere $S(R)$. Thus, here, the ADD stationary path does not intersect $S(R)$, i.e., the ADD stationary path is not transverse to $S(R)$. In this case, along the radial direction, a couple of ADD stationary paths emerge or disappear at $\overline{\boldsymbol{Q}}$. Saddle-node bifurcation[48] is one such bifurcation (see Fig. 5). Note that there is no ADD stationary path connecting the saddle-node bifurcation point and EQ (the origin). Thus, if only ADD stationary paths intersecting the EQ are followed, the TS located at $(x, y) = (-3.035, -10.776)$ should be overlooked. Saddle-node bifurcation in the GEF method, which is also unfavorable for reaction path search, was also reported.[52,53]

Hysteresis loop shown in Fig. 3c is also categorized into this type of bifurcation.

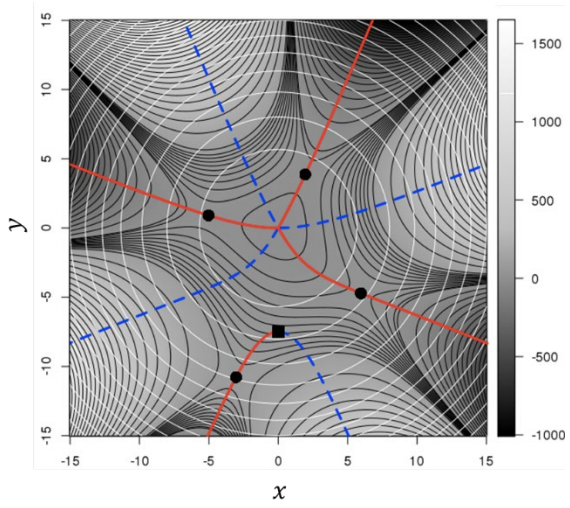

Figure 5. Saddle-node bifurcation: Model potential is given by $f(x,y) = x^2 + y^2 + 0.1(x^3 - 3xy^2) + 0.04(x^3y - xy^3)$. The origin is the minimum (EQ). The black solid curves and white circles represent the contours of $f(x,y)$ and those of the harmonic potential. TSs are shown by black circles, located at (*x*, *y*) = (5.960, -4.715), (1.951, 3.870), (-3.035, -10.776), (-5.022, 0.911). The ADD maximum and minimum paths are shown by red and blue dashed curves, respectively. A pair of ADD stationary paths emerge at the saddle-node bifurcation point, shown by a black square located at $(x,y) = (0,-7.5)$.

(CASE 3) Crossing point of paths: $h_\mu,\ b_\mu \neq 0\ (\mu = 1,\dots,r)$ and $h_\mu,\ b_\mu = 0\ (\mu = r+1,\dots,f-1)$

In this case, Eq. (28) or Eq. (22) is not sufficient to determine $d\overline{\boldsymbol{Q}}$. Let $\mathrm{rank}A = r\ (< f-1)$. Then, by applying Gaussian elimination to Eq. (28), Eq. (28) can be rewritten as

$$\begin{bmatrix} D_r \\ O_{f-1-r} \end{bmatrix} d\overline{\boldsymbol{Q}} = \mathbf{0}, \qquad (35)$$

where D_r is $r \times f$ matrix with $\mathrm{rank}\, D_r = r$. O_{f-1-r} is $(f-1-r) \times f$ zero matrix. The general solution of Eq. (35) is given by

$$d\overline{\boldsymbol{Q}} = \sum_{i=1}^{f-r} c_i \boldsymbol{v}_i, \qquad (36)$$

where $\boldsymbol{v}_i\ (i = 1,\dots,f-r)$ are orthonormal vectors that satisfy $D_r\boldsymbol{v}_i = \mathbf{0}$ and $c_i\ (i = 1,\dots,f-r)$ are coefficients. To determine the direction of $d\overline{\boldsymbol{Q}}$, i.e., to determine the ratio of c_i, higher-order derivatives of Eq. (22) or Eq. (28) are necessary. The second-order derivative of Eq. (22), i.e., the first-order derivative of Eq. (28), is given by

$$d(Ad\overline{\boldsymbol{Q}}) = Ad^2\overline{\boldsymbol{Q}} + \langle d\overline{\boldsymbol{Q}}, \frac{\partial A}{\partial \overline{\boldsymbol{Q}}} \rangle d\overline{\boldsymbol{Q}} = \mathbf{0}. \qquad (37)$$

By Gaussian elimination of A in Eq. (37), Eq. (37) can be rewritten as

$$\begin{bmatrix} D_r \\ O_{f-1-r} \end{bmatrix} d^2\overline{\boldsymbol{Q}} + \begin{bmatrix} E_r(d\overline{\boldsymbol{Q}}) \\ F_{f-1-r}(d\overline{\boldsymbol{Q}}) \end{bmatrix} d\overline{\boldsymbol{Q}} = \mathbf{0}, \qquad (38)$$

where $E_r(d\overline{\boldsymbol{Q}})$ and $F_{f-1-r}(d\overline{\boldsymbol{Q}})$ are $r \times f$ matrix and $(f-1-r) \times f$ matrix, the elements of which are all linear in $d\overline{\boldsymbol{Q}}$. The direction of $d\overline{\boldsymbol{Q}}$ might be determined by

$$\begin{cases} D_r d\overline{\boldsymbol{Q}} = \mathbf{0} \\ F_{f-1-r}(d\overline{\boldsymbol{Q}}) d\overline{\boldsymbol{Q}} = \mathbf{0} \end{cases}. \qquad (39)$$

However, there might be a case in which even higher-order derivatives of Eq. (28) are necessary to determine the direction of $d\overline{\boldsymbol{Q}}$. Since Eq. (39) are nonlinear equations, there may be more than one solution. Each real solution corresponds to a tangent vector of the ADD stationary path intersecting $\overline{\boldsymbol{Q}}$. Thus, when there are more than one real solutions, $\overline{\boldsymbol{Q}}$ is a bifurcation point and some ADD stationary paths intersect. Pitchfork bifurcation and transcritical bifurcation shown in Fig. 3 are categorized into this type of bifurcation. Pitchfork bifurcation is an example of bifurcation described in CASE 3

(see Fig. 6). Pitchfork bifurcation points can be found by following the ADD saddle paths intersecting the EQ. As shown in Fig. 4, the ADDF method does not necessarily follow the ADD saddle path leading to the pitchfork bifurcation point. Thus, the ADD maximum path caused by pitchfork bifurcation might be overlooked.

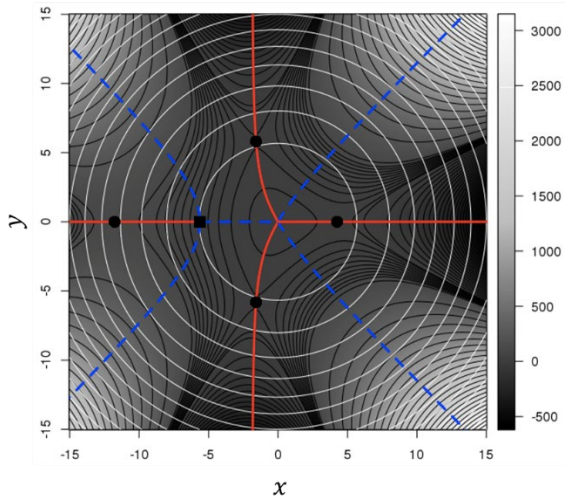

Figure 6. Pitchfork bifurcation: Model potentials are given by $f(x,y) = x^2 + y^2 - 0.1(x^3 - 3xy^2) - 0.01(x^4 - 6x^2y^2 + y^4)$. The origin is the minimum (EQ). The black curves represent the contours of $f(x,y)$. TSs are shown by black circles, located at $(x,y) = (4.254,0), (-1.577, \pm 5.814), (-11.754,0)$. At the pitchfork bifurcation point, shown by a black square located at $(x,y) = (-5.625,0)$, the ADD maximum path bifurcates, resulting in one minimum path and two maximum paths.

(CASE 4) Crossing of all paths tangent to the hypersphere: $\mathrm{rank}(Hess) < \mathrm{rank}(A)$, $\mathrm{rank}(Hess) \leq f - 3$

In this case, $\langle \boldsymbol{n}, d\overline{\boldsymbol{Q}} \rangle = 0$ and some ADD stationary paths intersect at $\overline{\boldsymbol{Q}}$. Eventually, the necessary condition for $\overline{\boldsymbol{Q}}$ to be a bifurcation point of the ADD stationary path is given by

$$\det(Hess) = 0. \qquad (40)$$

This condition is the singularity of the Hessian matrix given by Eq. (21). Thus, bifurcation of ADD stationary paths occurs at the ADD stationary inflection point. It is obvious that CASE 2–CASE 4 satisfy Eq. (40).

Notably, bifurcation of the ADD stationary path and that of the gradient extremal path are essentially the same phenomenon. The gradient extremal path is the curve connecting the stationary points of the norm of the energy gradient on the potential energy isosurfaces. Similarly, the ADD stationary paths are curves connecting the stationary points of ADD on the harmonic potential isosurfaces. As shown above, bifurcation of the ADD stationary path occurs only at the nonregular point of the Hessian matrix of the ADD function on the harmonic potential isosurfaces. In fact, the bifurcation of the gradient extremal path occurs at the nonregular point of the Hessian matrix of the energy gradient norm on the potential energy isosurfaces.[17,21]

The relation between ADDF and the distinguished coordinate method should be noted. The distinguished coordinate method follows only minimum energy point on the hyperplane perpendicular to the selected direction (see "Introduction"), and other stationary points are not followed. If the harmonic potential isosurface is used for constraint instead of the hyperplane, only ADD maximum paths are followed in the procedure of the distinguished coordinate. This is almost the same to ADDF, although the IOE technique follows some additional points other than ADD maxima. Thus, as RGF or NTs improved the distinguished coordinate, continuous trace of ADD stationary points, not only ADD maxima, seems to improve ADDF. At least, overlooking by bifurcation will be prevented, to some extent. This requires additional computational cost, of course.

ADD Inflection Paths

As discussed above, the ADD stationary paths bifurcate at the nonregular point of the Hessian matrix on hyperspheres, and thus, some of bifurcation points may be found by following the ADD inflection points. The IOE method follows not only ADD maxima but also ADD inflection-like points.[36,50] When only ADD maxima are followed, bifurcation of the ADD stationary paths is sometimes overlooked. Thus, following the ADD inflection points is important to reduce the risk of overlooking of the TSs. In this section, we show that the saddle-node bifurcation point shown in Fig. 5 can be found by following the ADD inflection paths, which are the curves generated by connecting the ADD inflection points.

First, we define the ADD inflection paths. Let $\bar{\boldsymbol{Q}}$ be an ADD non-stationary inflection point. Then, there is a zero eigenvalue of the Hessian matrix:

$$Hess(\bar{\boldsymbol{Q}})\boldsymbol{l}_1 = \boldsymbol{0}, \tag{41}$$

and

$$\sum_{\mu=1}^{f-1}(\boldsymbol{l}_\mu \otimes \boldsymbol{l}_\mu)\frac{\partial V_{\mathrm{ADD}}}{\partial \bar{\boldsymbol{Q}}}(\bar{\boldsymbol{Q}}) = \langle \boldsymbol{l}_1, \frac{\partial V_{\mathrm{ADD}}}{\partial \bar{\boldsymbol{Q}}}(\bar{\boldsymbol{Q}})\rangle \boldsymbol{l}_1 \tag{42}$$

hold. When $\bar{\boldsymbol{Q}}$ is an ADD stationary inflection point, Eq. (38) becomes obvious because $\langle \boldsymbol{l}_\mu, \frac{\partial V_{\mathrm{ADD}}}{\partial \bar{\boldsymbol{Q}}}(\bar{\boldsymbol{Q}})\rangle = 0 \quad (\mu = 1, \ldots, f-1)$. The curves that satisfy Eqs. (41) and (42) identically are called ADD inflection paths. Figure 7 shows the ADD inflection paths of the same potential as that shown in Fig. 5. Since there is no ADD maximum path that connects the saddle-node bifurcation point and EQ, it seems difficult to find the ADD maximum path appearing at the bifurcation point. However, if the ADD inflection path given by $x = 0$ is followed, the ADD maximum path could be found. Although what the IOE method follows in addition to the ADD maximum point is not an accurate ADD inflection point, the possibility to find the saddle-node bifurcation point might be enhanced. Accurate ADD inflection points defined by Eqs. (41) and (42) can be obtained by computing the stationary points of the norm of tangential components of ADD gradient on hyperspheres. This is related to the fact that gradient minimization affords not only stationary points but also minima of the gradient norm with a nonzero value.[4,52-56] The nonzero gradient minima satisfy only Eqs. (41) and (42). However, it is not practical to trace all the ADD inflection paths. Similar to the above discussion of the maximum number of ADD stationary paths, the maximum number of ADD inflection paths and ADD stationary paths is given by $\left(5^f - 1\right)/2$. This is confirmed as follows. The norm of the tangential components of ADD gradient on hyperspheres is given by $g = \langle \frac{\partial V_{\mathrm{ADD}}}{\partial \bar{\boldsymbol{Q}}}(\bar{\boldsymbol{Q}}), \left(I - \frac{\bar{\boldsymbol{Q}}\otimes\bar{\boldsymbol{Q}}}{\langle \bar{\boldsymbol{Q}},\bar{\boldsymbol{Q}}\rangle}\right)\frac{\partial V_{\mathrm{ADD}}}{\partial \bar{\boldsymbol{Q}}}(\bar{\boldsymbol{Q}})\rangle$. Since $\langle \bar{\boldsymbol{Q}}, \bar{\boldsymbol{Q}}\rangle$ is constant on a hypersphere, the stationary point of g is identical to that of $\langle \bar{\boldsymbol{Q}}, \bar{\boldsymbol{Q}}\rangle \langle \frac{\partial V_{\mathrm{ADD}}}{\partial \bar{\boldsymbol{Q}}}(\bar{\boldsymbol{Q}}), \left(I - \frac{\bar{\boldsymbol{Q}}\otimes\bar{\boldsymbol{Q}}}{\langle \bar{\boldsymbol{Q}},\bar{\boldsymbol{Q}}\rangle}\right)\frac{\partial V_{\mathrm{ADD}}}{\partial \bar{\boldsymbol{Q}}}(\bar{\boldsymbol{Q}})\rangle$. The lowest degree of the Taylor expansion of $\langle \bar{\boldsymbol{Q}}, \bar{\boldsymbol{Q}}\rangle g$ is 6. The maximum number of stationary points of homogeneous polynomial of n variables with a degree of $m(\geq 3)$ on a hypersphere centered at the origin is given by $2\{(m-1)^n - 1\}/(m-2)$ when the number of stationary points is finite.[44] Thus, the maximum number of ADD inflection paths and stationary paths given above is obtained.

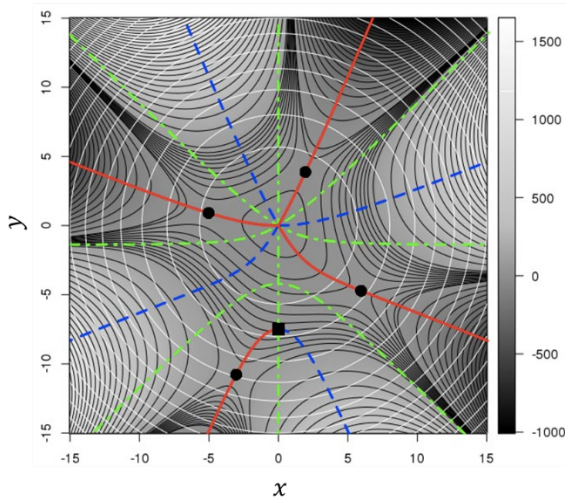

Figure 7. ADD inflection paths (green dot-dash curves) determined on the model potential (the same as in Fig. 5). The saddle-node bifurcation point and the origin (EQ) are connected by the ADD inflection path given by $x = 0$.

Completeness of TS Search by ADDF Method

As discussed in the section "ADDF Method", the ADDF method seems to be able to find all the TSs from the minimum if all the ADD stationary paths and ADD inflection paths were followed. Figure 8 shows the schematic of typical bifurcations of ADD stationary paths. All the TSs shown in the four panels can be located by tracing ADD stationary paths and inflection paths. However, there is a different type of bifurcation of the ADD stationary path at which all the ADD stationary paths and ADD inflection paths are tangent to the hypersphere. This indicates that, there is a type of bifurcation point at which the tangent vectors of ADD stationary paths and ADD inflection paths are all tangent to the hypersphere and none of these paths intersects any EQ. ADD maximum paths generated by this bifurcation may not be found even if all the ADD stationary paths and ADD inflection paths intersecting the EQ are followed. The proof for the existence of such a type of bifurcation is given in Supporting Information.

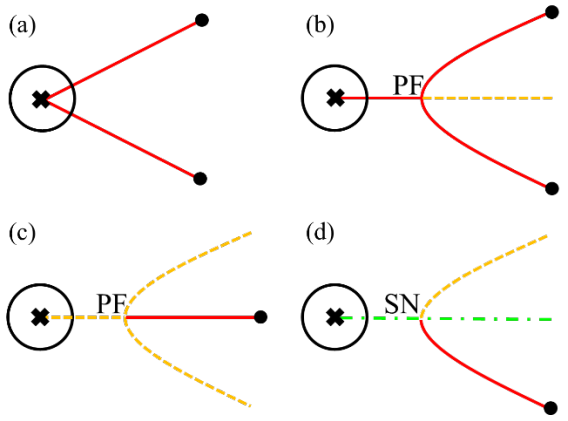

Figure 8. Schematic of typical bifurcations of ADD stationary paths. The red curves and the yellow dashed curves denote the ADD maximum paths and ADD saddle paths, respectively, while the green dot-dash line denotes the ADD inflection path. Black crosses and circles indicate EQs and TSs, and the circles around the EQs show the initial hyperspheres of the ADDF method. (a) Both of the two ADD maximum paths intersect with the initial hypersphere; (b) the ADD maximum path intersecting with the initial hypersphere bifurcates at the pitchfork (PF) bifurcation point; (c) the ADD maximum path appears at the PF bifurcation point; and (d) the ADD maximum path appears at the saddle-node (SN) bifurcation point.

Conclusions

In this paper, we report a detailed investigation of the mathematical aspect of the ADD stationary path. We first confirmed that the maximum number of the ADD stationary paths intersecting the EQ is given by $2^{f+1} - 2$, where f is the degree of freedom of the system. Next, the bifurcation of the ADD stationary path was discussed. Typical bifurcations like saddle-node bifurcation and pitchfork bifurcation are possible.

Although the IOE method was originally introduced to detect the ADD maximum direction on the initial hypersphere even for bifurcation, it does not always work as expected. We showed the case in which only ADD maxima of the original potential are followed and the technique fails to detect the bifurcation. However, the idea to follow not only ADD maxima but also ADD inflection points is important to reduce the risk of overlooking of the bifurcation. We demonstrated a case where following the ADD inflection points leads to finding the ADD maxima generated on the way by saddle-node bifurcation. However, unfortunately, the ADDF method cannot ensure that all the TSs will be found because there is another type of bifurcation in which the tangent vectors of all the ADD stationary paths and ADD inflection paths are tangent to the hypersphere and none of these paths intersects any EQ point. To improve the completeness of the reaction path search by the ADDF method, management of the bifurcation of the ADD stationary path is essential.

Acknowledgments

SE was supported by the Institute for Quantum Chemical Exploration through the Research Fellowship for Young Scientists. TT (Tsutsumi) was supported by the Ministry of Education, Culture, Sports, Science and Technology (MEXT, Japan) through Program for Leading Graduate Schools (Hokkaido University "Ambitious Leader's Program") and Grant-in-Aid for Japan Society for the Promotion of Science (JSPS, Japan) Fellows Grant Number JP18J20856. This work was partly supported by JST CREST Grant Number JPMJCR1902, the MEXT program "Elements Strategy Initiative to Form Core Research Center" (since 2012), and the Photo-excitonix Project in Hokkaido University. A part of calculations was performed using the Research Center for Computational Science, Okazaki, Japan.

Keywords:

Anharmonic downward distortion, Reaction path, Bifurcation, Potential energy surface, Transition state

Additional Supporting Information may be found in the online version of this article.

References and Notes

1. Fukui, K., *J. Phys. Chem.* **1970**, *74*, 4161-4163.
2. Fukui, K., *Acc. Chem. Res.* **1981**, *14*, 363-368.
3. Maeda, S., Y. Harabuchi, Y. Ono, T. Taketsugu, K. Morokuma, *Int. J. Quantum Chem.* **2015**, *143*, 258-269.
4. Schlegel, H. B., *Wiley Interdiscip. Rev. Comput. Mol. Sci.* **2011**, *1*, 790-809.
5. Jónsson, H.; Mills, G.; Jacobsen, W. In Classical and Quantum Dynamics in Condensed Phase Simulations; Berne, B. J.; Cicotti, G.; Coker, D. F., Eds.; World Scientific, Singapore, **1998**; Chapter 16, pp 385-404.
6. Rothman, M. J., Lohr Jr, L. L., *Chem. Phys. Lett.* **1980**, *70*, 405-409.
7. Scharfenberg, P., *Chem. Phys. Lett.* **1981**, *79*, 115-117.
8. Williams, I. H., Maggoria, G. M., *J. Mol. Struct.* (*Theochem.*) **1982**, *89*, 365-378.
9. Burkert, U., Allinger, N. L., *J. Comput. Chem.* **1982**, *3*, 40-46.
10. Bauschlicher, C. W., Schaefer III, H. F., Bender, C. F., *J. Am. Chem. Soc.* **1976**, *98*, 1653-1658.
11. Pancíř, J., *Collect. Czech. Chem. Commun.* **1975**, *40*, 1112-1118.
12. Basilevsky, M. V., Shamov, A. G., *Chem. Phys.* **1981**, *60*, 347-358.
13. Basilevsky, M. V., *Chem. Phys.* **1982**, *67*, 337-346.
14. Rowe, D. J., Ryman, A., *J. Math. Phys.* **1982**, *23*, 732-735.
15. Hoffman, D. K., Nord, R. S., Ruedenberg, K., *Theor. Chim. Acta* **1986**, *69*, 265-279.

16. Jørgensen, P., Jensen, H. J. A., Helgaker, T., *Theor. Chim. Acta* **1988**, *73*, 55-65.
17. Quapp, W., *Theor. Chim. Acta* **1989**, *75*, 447-460.
18. Shida, N., Almlöf, J. E., Barbara, P. F., *Theor. Chim. Acta* **1989**, *76*, 7-31.
19. Schlegel, H. B., *Theor. Chim. Acta* **1992**, *83*, 15-20.
20. Sun, J.-Q., Ruedenberg, K., *J. Chem. Phys.* **1993**, *98*, 9707-9714.
21. Bondensgård, K., Jensen, F., *J. Chem. Phys.* **1996**, *104*, 8025-8031.
22. Quapp, W., Hirsch, M., Imig, O., Heidrich, D., *J. Comput. Chem.* **1998**, *19*, 1087-1100.
23. Quapp, W., Hrisch, M., Heidrich, D., *Theor. Chem. Acc.* **1998**, *100*, 285-299.
24. Hirsch, M., Quapp, W., Heidrich, D., *Phys. Chem. Chem. Phys.* **1999**, *1*, 5291-5299.
25. Quapp, W., *J. Theor. Comput. Chem.* **2003**, *2*, 385-417.
26. Quapp, W., Hirsch, M., Heidrich, D., *Theor. Chem. Acc.* **2004**, *1*, 40-51.
27. Hirsch, M., Quapp, W., *J. Mol. Strcut.* (*Theochem.*) **2004**, *683*,1-13.
28. Hirsch, M., Quapp, W., *Chem. Phys. Lett.* **2004**, *395*, 150-156.
29. Quapp, W., *J. Math. Chem.* **2004**, *36*, 365-379.
30. Bofill, J. M., Quapp, W., *J. Chem. Phys*. **2011**, *134*, 074101.
31. Quapp, W., Bofill, J. M., Caballero, M., *Chem. Phys. Lett.* **2012**, *541*, 122-127.
32. Ohno, K., Maeda, S., *Chem. Phys. Lett.* **2004**, *384*, 277-282.
33. Maeda, S., Ohno, K., *J. Phys. Chem. A* **2005**, *109*, 5724-5753.
34. Maeda, S., Ohno, K., *Chem. Phys. Lett.* **2008**, *460*, 55-58.
35. Maeda, S., Ohno, K., Morokuma, K., *J. Phys. Chem. A* **2009**, *113*, 1704-1710.
36. Maeda, S., Ohno, K., Morokuma, K., *Phys. Chem. Chem. Phys.* **2013**, *15*, 3683-3701.
37. Maeda, S., Taketsugu, T., Morokuma, K., Ohno, K., *Bull. Chem. Soc. Jpn.* **2014**, *87*, 1315.
38. Kodaya, Y., Oki, T., Yamakado, H., Tokoyama, H., Ohno, K., *Chem. Lett.* **2019**, *48*, 1288-1291.
39. Mitsuta, Y., Käster, J., Yamataka, S., Kawakami, T., Okumura, M., *Mol. Phys*. **2019**, *117*, 2284-2292.
40. Mitsuta, Y., Shigeta, Y., *J. Chem. Theory Comput.* **2020**, DOI: 10.1021/acs.jctc.0c00010.
41. Maeda, S., Osada, Y., Taketsugu, T., Morokuma, K., Ohno, K., GRRM14, http://iqce.jp/GRRM/index_e.shtml
42. Kuznetsov, É. D., Kholshevnikov, K. V., *Sov. Astron.* **1992**, *36*, 220-222.
43. Ni, G., Qi, L., Wang, F., Wang, Y., *J. Math. Anal. Appl.* **2007**, *329*, 1218-1229.
44. Cartwright, D., Sturmfels, B., *Linear Algebra Appl.* **2013**, *438*, 942-952.
45. Hirsch, Quapp and Heidrich observed RGF paths in H_2O (Ref. 24).
46. Auzinger, W., Stetter, H. J., *Internat. Schriftenreihe Numer. Math.*, **1988**, *86*, 11-30.
47. Frisch, M. J., Trucks, G. W., Schlegel, H. B., Robb, B. M. M. A., Cheeseman, J. R., Scalmani, G., Barone, V., Petersson, H. P. H. G. A., Nakatsuji, H., Caricato, M., Li, X., Izmaylov, M. H. A. F., Bloino, J., Zheng, G., Sonnenberg, J. L., Ehara, T. N. M., Toyota, K., Fukuda, R., Hasegawa, J., Ishida, M., Honda, J. Y., Kitao, O., Nakai, H., Vreven, T., Montgomery, J. A., Peralta, E. B. J. E., Ogliaro, F., Bearpark, M., Heyd, J. J., Kudin, J. N. K. N., Staroverov, V. N., Keith, T., Kobayashi, R., Raghavachari, J. T. K., Rendell, A., Burant, J. C., Iyengar, S. S., Cossi, J. B. C. M., Rega, N., Millam, J. M., Klene, M., Knox, J. E., Bakken, R. E. S. V., Adamo, C., Jaramillo, J., Gomperts, R., Yazyev, J. W. O. O., Austin, A. J., Cammi, R., Pomelli, C., Martin, G. A. V. R. L., Morokuma, K., Zakrzewski, V. G., Salvador, A. D. D. P., Dannenberg, J. J., Dapprich, S., Farkas, J. C. O., Foresman, J.

B., Ortiz, J. V., and Fox, D. J., Gaussian 09, Revision D.01. Gaussian, Inc., Wallingford CT, **2013**.
48. Strogatz, S. H. Nonlinear dynamics and chaos : with applications to physics, biology, chemistry, and engineering; Westview Press, Cambridge Massachsetts, USA, **2000**.
49. Some other TS geometries are obtained by ADDF method in GRRM14 program (the options UpDC and DownDC, parameters to recognize dissociation channels, were set large enough so as TS geometries with long bond length to be found). However, their absolute values of imaginary frequencies are too small and interatomic distances between fragments are too large (> 3 Å).
50. Maeda, S., Private communication.
51. Weatherburn, C. E. An introduction to Riemannian geometry and tensor calculus; Cambridge University Press, Cambridge, UK, **1938**.
52. Müller, K., *Angew. Chem.* (*Int. Ed. Engl.*) **1980**, *19*, 1-13.
53. Schlegel, H. B., *J. Comput. Chem.* **2003**, *24*, 1514-1527.
54. McIver, J. W., Komornicki, A., *J. Am. Chem. Soc.* **1972**, *94*, 2625-2633.
55. Poppinger, D., *Chem. Phys. Lett.* **1975**, *35*, 550-554.
56. Komornicki, A., Ishida, K., Morokuma, K., Ditchfield, R., Conrad, M., *Chem. Phys. Lett.* **1977**, *45*, 595-602.

GRAPHICAL ABSTRACT

The anharmonic downward distortion following (ADDF) method explores transition states from potential minimum by tracing ADD maximum points on the hypersphere centered at the minimum. This paper clarified the maximum number of ADD stationary paths intersecting the minimum and the necessary condition for the bifurcation of ADD stationary paths. The ADDF computations were demonstrated for a H_2O molecule.